Доклади на Българската академия на науките
Comptes rendus de l'Académie bulgare des Sciences

Tome 76, No 4, 2023

GEOPHYSICS

Seismology

DETERMINING THE DEFORMATIONS OF THE EARTH'S SURFACE AFTER THE EARTHQUAKES IN TURKEY-SYRIA OF 06 FEBRUARY 2023 – INITIAL RESULTS

Mila Atanasova[#], Plamena Raykova, Hristo Nikolov*

Received on March 8, 2023
Presented by D. Solakov, Corresponding Member of BAS, on March 28, 2023

Abstract

Two devastating earthquakes of magnitude M_W 7.8 and M_W 7.5 hit Turkey on February 6, 2023. The earthquakes occurred in the East Anatolian Fault Zone, westwards of Gaziantep, Turkey. The quake was followed by intensive aftershock activity. This study presents initial results from interferometric processing of SAR data from the European Space Agency Sentinel-1 mission revealing the affected area and the magnitude of the deformations that occurred after the earthquakes. The produced maps are combination of data from several sources. Data of the epicenters of the events are from EMSC[1], and the active faults are from EDAF[2], both considered to be the driving forces of these ground movements. SAR data were used to produce information showing the actual surface displacements. It needs to be highlighted that the said information reflects not the consequences of the single seismic event but the effect of all earthquakes that took place in the investigated region between the dates of registration by the SAR instrument. In this paper, the presented results are only part of the larger set of interferograms and maps of the derived from them vertical displacements.

Key words: earthquakes, deformation, InSAR

[#]Corresponding author.

DOI:10.7546/CRABS.2023.04.07

[1]European-Mediterranean Seismological Centre

[2]European Database of Seismogenic Faults

Introduction. The territory of Turkey represents a typical example of a high seismic risk zone. Turkey is located between three large tectonic plates. In terms of earthquake activity, this area is one of the most active areas. The observed earthquakes are result of the collision of the Arabian and African plates with Eurasia. Although the plates have different sizes in the region based on the spatial distribution of seismicity, mostly three plate boundaries have an important role – the African, Arabian, and Eurasian plates. The African and Arabian plates to the south, and the Eurasian plate to the north, surround the Anatolian plate, where Turkey is located. The movements between these three plates are the reason for most of the activity in the region. For that reason, the Anatolian plate has high seismicity. The Anatolian plate involves the North Anatolian Fault Zone (NAFZ), the East Anatolian Fault Zone (EAFZ), and the Southeast Anatolian Thrust Zone (SAT), which form the boundaries of the plate and the important active fault segments throughout Western Anatolia [1].

The East Anatolian Fault Zone is one of the most significant elements in this tectonic area, outlining a left-lateral strike-slip plate boundary extending between the Arabian and Anatolian plates in eastern Turkey. The proceeded northward migration of the Arabian plate with respect to stable Eurasia since the Miocene resulted in the westward extrusion of the Anatolian plate along the North and East Anatolian Fault Zones, respectively [2]. This structure presents a plate boundary expanding over 500 km between the Arabian and Anatolian plates [3]. The observed plate motion, with slip rates varying from 6 to 10 mm/yr, has resulted in destructive earthquakes in eastern Turkey, as documented by historical records.

In 1969 Allen [4], first defined the EAFZ, and according to other authors [5], this structure extends from the Karliova triple junction, where it attaches the North Anatolian Fault Zone to the southwest for about 600 km to the Kahramanmaras triple junction near Antakya. The fault zone attaches to another fault structure – the Dead Sea Fault Zone [6]. There is data that the structure was formed between the Late Miocene and Early Pliocene [6].

There is a historical record of destructive $M > 7$ earthquakes in eastern Turkey as a consequence of sliding along the fault. In the last century, only one major earthquake was recorded around the structure (on December 4, 1905; $M = 6.8$) [7]. Historical and instrumental records show major differences between historical and current seismicity, respectively. The main known earthquakes in the area occurred on November 29, 1114 ($M > 7.8$), March 28, 1513 ($M > 7.4$), and March 2, 1893 ($M > 7.1$), respectively [8]. Çetin et al. [9] considered apparent seismic attenuation throughout the zone to indicate the possibility that the fault is currently locked.

Figure 1 presents earthquakes with moment magnitude $M_W \geq 4.0$ generated in the Anatolia region during the period 1900 to 2012 and active faults of Turkey, where the North Anatolian Fault Zone and the Eastern Anatolian Fault Zone are illustrated (in that zone the main earthquakes with M_W 7.8 are registered).

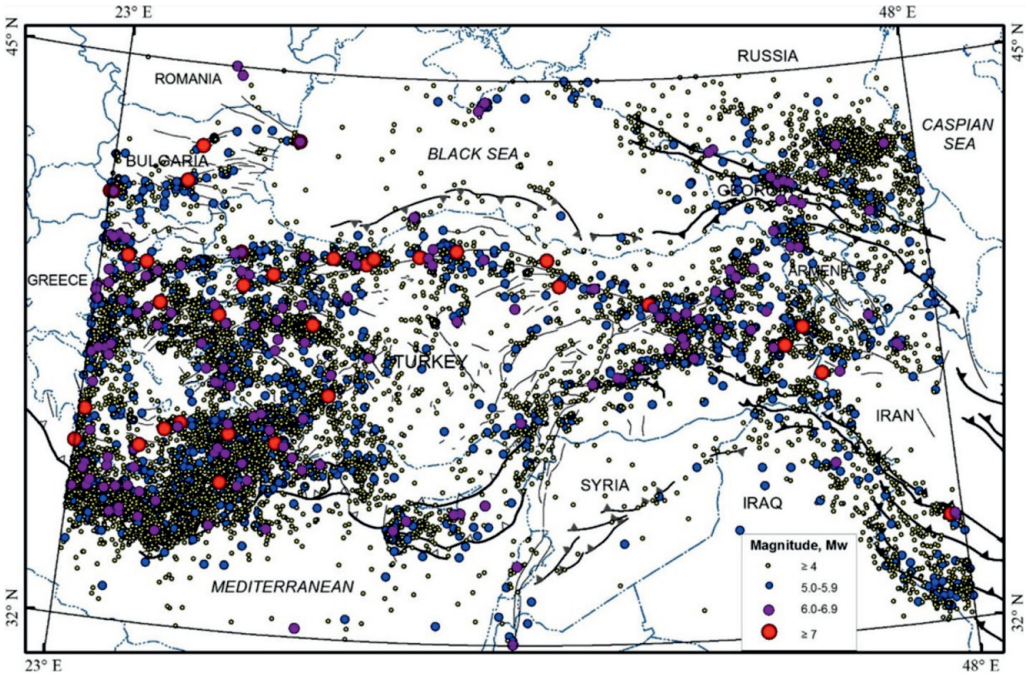


Fig. 1. Spatial distribution of recent seismicity in the Anatolia region during the period 1900 to 2012 [10]

On February 6, 2023, an earthquake of M_W 7.8 hit The East Anatolian Fault Zone [11]. The earthquake epicenter was located westwards of the city of Gaziantep, Turkey, and its focal depth reveals a shallow event. The earthquake was largely felt on the territory of Turkey and neighbouring countries: Greece, Bulgaria, Romania, and Croatia. The main shock triggered a destructive aftershock within the same fault zone, at a distance of 100 km further north with moment magnitude M_W 7.5. These earthquakes caused extensive primary and secondary effects on the environment, including surface ruptures, ground cracks, liquefaction phenomena, and hydrological anomalies, causing extensive impacts on networks and infrastructure [12]. For one week after the main earthquake, the aftershock sequence included more than 3400 seismic events.

Ten days after earthquake, the Disaster and Emergency Management Presidency (AFAD) has reported 38 044 human casualties, while over 160 000 people have been evacuated from the 10 earthquake-affected provinces. In Syria, over 5000 human casualties have been reported and these numbers are expected to increase as the search and rescue operations have reached their completion [12].

Utkucu et al. [13] considered the stress background of the 2023 earthquakes to search for stress interactions of those earthquakes with the earthquakes in the past. Coseismic stress change calculations indicate that the stress changes caused by the earthquake with magnitude M_W 7.8 is considered to rupture the 1114,

1513, and 1822 earthquake rupture segments and triggered event with magnitude M_W 7.5, estimated to rupture the 1544 earthquake rupture segments.

Method. The Differential Interferometry Synthetic Aperture Radar (DInSAR) technique was used to produce the results provided in this paper. Implementing it the vertical ground movements of an area of the studied event can be measured with centimeter accuracy. The source data for producing interferograms are from synthetic aperture radars (SAR), most often onboard satellites or planes. Those systems emit linearly polarized highly coherent electromagnetic waves at precise wavelength λ to the Earth's surface and register the signal backscattered from it. The time interval between sending and receiving the radar signal corresponds to the distance to the objects on the surface. This principle of the SAR data registration is presented in Fig. 2. It is seen that the SAR acquisition geometry is oblique, side-looking, with the look angle denoted by θ, which is the angle between the nadir and antenna line-of-sight (LOS) directions.

The SAR data registered by the instrument consists of a matrix with complex values of a single footprint area on the surface (also called a ground element). Thus, all footprints in range and azimuth directions form an image. The real part of a single matrix element corresponds to the amplitude of the reflected signal, while the imaginary part represents the phase of it. In order to process the SAR data further their preliminary processing is an essential step, which performs internal calibration, takes into account the Doppler shifts, improves the spatial resolution in range and azimuth. It should be pointed out that single complex

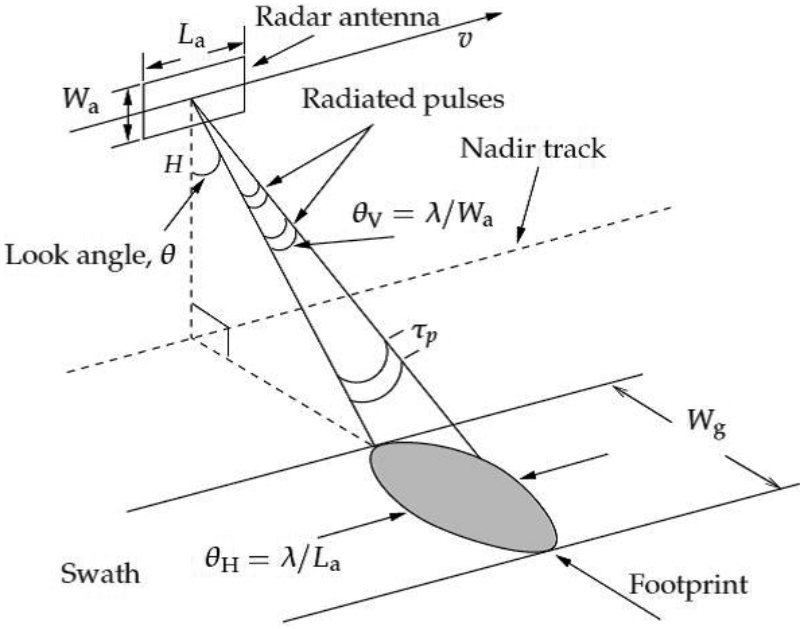


Fig. 2. Geometry of SAR data acquisition (as in [14])

SAR image cannot provide any useful information about the position of the objects within the ground element. To obtain the difference in position of the said objects, two images from almost the same position of the satellite denoted by H are needed to form an interferometric image, but from different dates. This new image delivers information for the deformations occurred on the surface in this time interval in LOS of the antenna, but in it, there is a part that reflects the underlying topography, too. The contribution of the underlying terrain in the phase signal is removed by creating a differential interferogram between the registered values and an interferogram computed from an external digital elevation model. A crucial step in obtaining the values for the occurred surface displacements is the transformation of the phase values from $[-\pi; \pi]$ interval to multiples of π known as phase unwrapping. Since this procedure is not straightforward, fine-tuning its parameters in several iterations is necessary. After the unwrapping conversion, the integer multiples of π should be transformed into metric unit displacements in the line of sight of the instrument. The last essential procedure is the transformation of the displacement map from radar geometry to a specific datum.

Data. In the framework of the present study, the SAR instrument located on board the Sentinel-1 satellite, maintained by the European Space Agency (ESA), registered the used data. The data is in the form of pre-processed and calibrated data products in Single look complex (SLC) format delivered by the ESAs' Instrument Processing Facility for further thematic processing. In those products, the included images have complex values that represent the amplitude and phase of the backscattered signals from the Earth's surface, which, together with the relevant metadata, form a single SAR product.

The produced information that reveals the deformation values is based on SAR data from the constellation consisting of two satellites (A and B) of the Sentinel-1 mission, which are freely distributed by ESA through a dedicated online data archive or other mirrored data repositories [15, 16]. Each satellite has a repeat-pass period of 12 days, meaning that the same part of the Earth's surface is imaged every 6 days by one of the two satellites, as they are 180° apart in the orbital plane. The main equipment of each of the two satellites is C-band radar (corresponding to an electromagnetic wave at 5.56 cm in length). The antenna of the instrument has right-oriented LOS regardless of the direction of the current orbit of the satellite – ascending or descending. The main mode for SAR data registration of Sentinel-1 is the Terrain Observation by Progressive Scans (TOPS).

Interferometric processing implies the usage of SAR data registered in Interferometric Wide (IW) mode and processed to SLC products since in this type of product, not only the amplitude of the signal reflected from the Earth's surface is included, but also its phase. The phase signal is crucial because, after appropriate processing, it provides information about changes in the distance to the observed objects from the Earth's surface to the position of a satellite at each pass over the investigated area [17, 18].

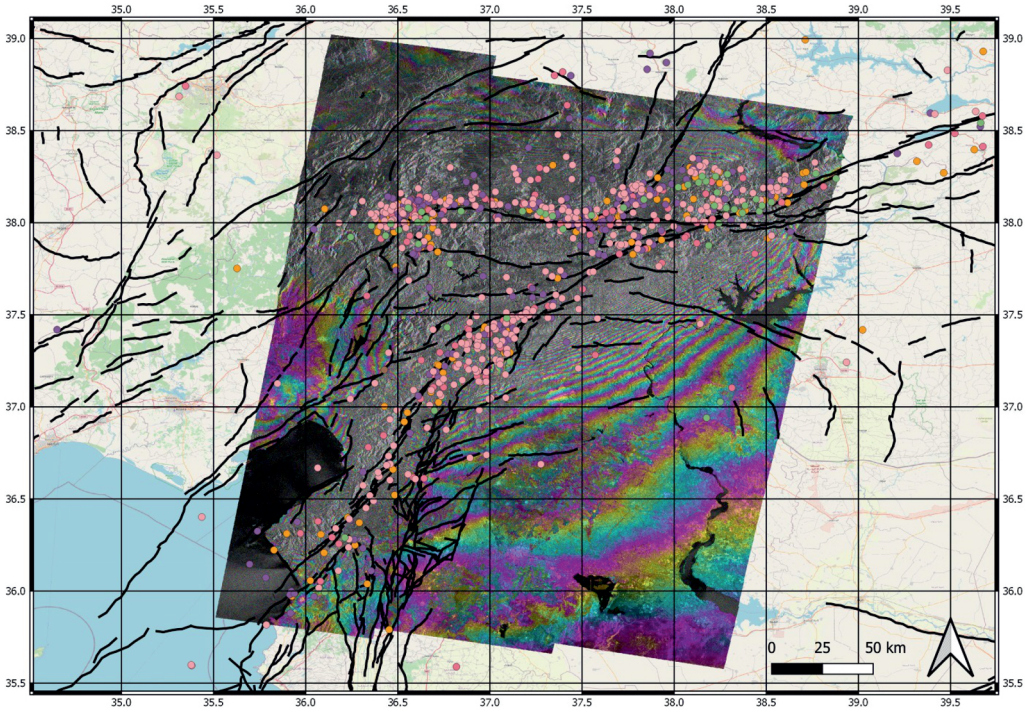


Fig. 3. The interferometric image from the descending orbit 21 track numbers from 29 Jan 2023 to 10 Feb 2023

In this research, SAR data from the tracking number of the descending orbit is 21, and the track numbers of the ascending orbits are 14 and 116 because the researched area was imaged by both tracks. The acquisition dates for orbit 21 span from January 29, 2023 to February 10, 2023. The interferogram presented in Fig. 3 was produced by DInSAR processing method. Since the data of ascending orbit 116 have not been provided in the ESA to the moment the paper was in preparation, they could not be processed together with those from orbit 14. This fact prevented to produce information that overlapped the study area where the studied event produced surface disruptions.

Results. In this paper, the deformations of the Earth's surface after the earthquake sequence from February 6, 2023 in Turkey were estimated via interferometric processing of SAR data. The produced results are in the form of wrapped interferometric images (see Fig. 3), where the interferometric fringes provide information about the displacements that have been produced by the event. It needs to be pointed out that each of the fringes corresponds to a displacement of 28 mm along the line of sight (LOS) of the satellite. The interferometric fringe is represented with a gradient of colours from a specific colour palette reaching the same colour from which it started – for example, from yellow to yellow. The density of the interferometric fringes for a single measurement unit (e.g., 50 km) in LOS reflects the displacements of the Earth's crust for this unit.

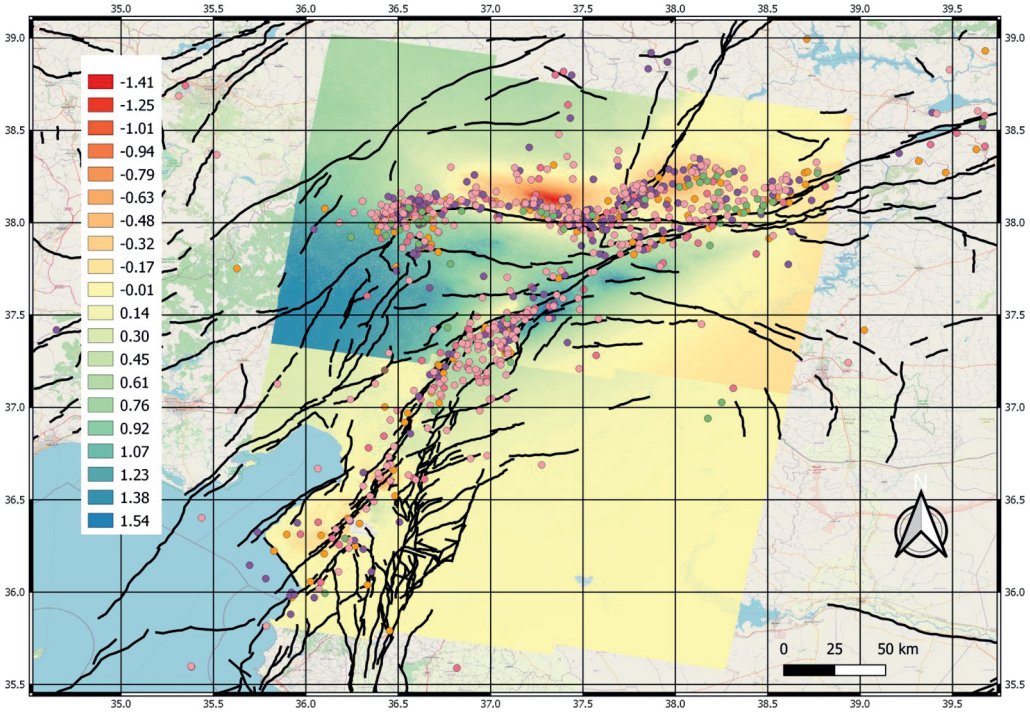


Fig. 4. Map of vertical displacements registered after the coseismic event on February 6 determined by the DInSAR technology

In order to demonstrate the origins of the studied event in Fig. 3 and Fig. 4, additional sources of data were used too. One of them is the main faults located in the zone being represented by black lines in the same figures [19], and as it is seen, the displacements registered from SAR data are concentrated in them. The points show the location of all earthquakes with a magnitude greater than 3.0 recorded by EMSC [20] during the period 06.02.2023–12.02.2023.

The interpretation of the results shows the vertical displacements (the colour scale in Fig. 4), which, expectedly, are concentrated in the areas around the main faults in the area.

Coseismic displacement of the February 6, 2023 earthquake by processing InSAR observations from C-band Sentinel-1 data along descending orbit was derived. The research interest, in this case, was provoked by the fact that the precise orbits of the satellite normally are made available by the authority managing the ground segment of the satellite for a wider audience about a month after the data acquisition, and until then only the restituted orbits are available. Multiple-looking geometry from InSAR helps in resolving displacement in the LOS of the earthquake and vertical deformations.

Conclusion. This study shows the initial results of the recorded ground deformations that occurred after the devastating earthquakes in Turkey and Syria

and the size and extent of the affected area determined by the DinSAR method. The interferometric phase and range pixel offset data completely cover the faults area that is based on the earthquakes. InSAR method facilitates mapping the surface of the earthquake faulting. The length of the surface rupture is found to be more than 350 km using InSAR observations because it falls along two SAR images. The InSAR technology provides an alternative tool to ground observation in the study of earthquake deformation. DInSAR is highly complementary to the ground observations in the field and covers the entire fault with good resolution and moderate precision.

REFERENCES

[1] Kalafat D., A. Zulfikar, S. Akcan (2021) Seismicity of Turkey and Real-Time Seismology Applications in Determining Earthquake Hazard, Academic Platform Journal of Natural Hazards and Disaster Management, **2**(2), 96–111, https://doi.org/10.52114/apjhad.1039670.

[2] Şengör A. M. C., O. Tüysüz, C. İmren, M. Sakinç, E. Eyidoğan et al. (2005) The North Anatolian Fault: A new look, Annu. Rev. Earth Planet. Sci., **33**, 37–112, https://doi.org/10.1146/annurev.earth.32.101802.120415.

[3] Bulut F., M. Bohnhoff, T. Eken, C. Janssen, T. Kiliç, G. Dresen (2012) The East Anatolian Fault Zone: Seismotectonic setting and spatiotemporal characteristics of seismicity based on precise earthquake locations, J. Geophys. Res., **117**, B07304, https://doi.org/10.1029/2011JB008966.

[4] Allen C. R. (1969) Active faulting in northern Turkey, Rep. 1577, 32 pp., Div. of Geol. Sic., Calif. Inst. of Technol., Pasadena.

[5] Over S., S. Ozden, H. Yilmaz (2004) Late Cenozoic stress evolution along the Karasu Valley, SE Turkey, Tectonophysics, **380**, 43–68, https://doi.org/10.1016/j.tecto.2003.11.011.

[6] Şengör A. M. C., N. Gorür (1985) Strike-slip faulting and related basin formation in zones of tectonic escape: Turkey as a case study. In: Strike-Slip Deformation, Basin Formation and Sedimentation, K. Biddle, N. Christie-Blick (Eds), Special Publications, SEPM Society for Sedimentary Geology, Tulsa, **37**, 227–264.

[7] Nalbant S. S., J. McCloskey, S. Steacy, A. A. Barka (2002) Stress accumulation and increased seismic risk in eastern Turkey, Earth Planet. Sci. Lett., **195**, 291–298, https://doi.org/10.1016/S0012-821X(01)00592-1.

[8] Ambraseys N. N., J. A. Jackson (1998) Faulting associated with historical and recent earthquakes in the Eastern Mediterranean region, Geophys. J. Int., **133**, 390–406, https://doi.org/10.1046/j.1365-246X.1998.00508.x.

[9] Çetin H., H. Güneyli, L. Mayer (2003) Paleoseismology of the Palu-Lake Hazar segment of the East Anatolian Fault Zone, Turkey, Tectonophysics, **374**, 163–197, https://doi.org/10.1016/j.tecto.2003.08.003.

[10] Duman T. Y., T. Çan, Ö. Emre, F. T. Kadirioğlu, N. B. Baştürk et al. (2016) Seismotectonics database of Turkey, Bull. Earthq. Eng., **16**, 3277–3316, https://doi.org/10.1007/s10518-016-9965-9.

[11] USGS NEIC (2023) https://earthquake.usgs.gov/earthquakes/eventpage/us6000jllz/executive.
[12] Lekkas E., P. Carydis, E. Vassilakis, S. Mavroulis, I. Argyropoulos et al. (2023) The February 6 2023 Turkey-Syria Earthquakes, Newsletter of Environmental, Disaster and Crises Management Strategies, **29**, ISSN 2653-9454, DOI: 10.13140/RG.2.2.17643.82726.
[13] Utkucu M., H. Durmuş, F. Uzunca, S. Nalbant (2023) A preliminary report on the 2023 Gaziantep (Mw=7.7) and Elbistan (Mw=7.5) Earthquakes in Southeast Türkiye, Sakarya University, Sakarya, Türkiye, https://doi.org/10.13140/RG.2.2.17088.40963.
[14] Lauknes T. R. (2004) Long-term surface deformation mapping using small-baseline differential SAR interferograms, Master Thesis, Department of Physics and Technology, University of Tromso, Norway.
[15] https://scihub.copernicus.eu/dhus/#/home.
[16] InSAR product by ASF DAAC HyP3 2023 (contains modified Copernicus Sentinel data 2023, processed by ESA).
[17] Ferretti A., A. Monti-Guarnieri, C. Prati, F. Rocca, D. Massonnet (2007) InSAR principles: guidelines for SAR interferometry processing and interpretation, ESA Publications, TM-19.
[18] Hanssen R. F. (2001) Radar interferometry: data interpretation and error analysis, Dordrecht, Netherlands, Kluwer Academic Publishers.
[19] Basili R., V. Kastelic, M. B. Demircioglu, D. Garcia Moreno, E. S. Nemser et al. (2013) The European Database of Seismogenic Faults (EDSF) compiled in the framework of the Project SHARE, https://doi.org/10.6092/INGV.IT-SHARE-EDSF.
[20] https://www.emsc-csem.org/Earthquake/271/Earthquake-sequence-in-Turkey-February-6th-2023.

National Institute of Geophysics,
Geodesy and Geography
Bulgarian Academy of Sciences
Akad. G. Bonchev St, Bl. 3
1113 Sofia, Bulgaria
e-mails: mila_at_zl@abv.bg
plamena.raikova@gmail.com

Space Research and Technology Institute
Bulgarian Academy of Sciences
Akad. G. Bonchev St, Bl. 1
1113 Sofia, Bulgaria
e-mail: hristo@stil.bas.bg